ADVANCED MATERIALS
www.advmat.de

Mechanism for Generating H_2O_2 at Water-Solid Interface by Contact-Electrification

Andy Berbille, Xiao-Fen Li, Yusen Su, Shunning Li, Xin Zhao, Laipan Zhu, and Zhong Lin Wang**

The recent intensification of the study of contact-electrification at water-solid interfaces and its role in physicochemical processes lead to the realization that electron transfers during water-solid contact-electrification can drive chemical reactions. This mechanism, named contact-electro-catalysis (CEC), allows chemically inert fluorinated polymers to act like single electrode electrochemical systems. This study shows hydrogen peroxide (H_2O_2) is generated from air and deionized water, by ultrasound driven CEC, using fluorinated ethylene propylene (FEP) as the catalyst. For a mass ratio of catalyst to solution of 1:10000, at 20 °C, the kinetic rate of H_2O_2 evolution reaches 58.87 mmol L^{-1} $g_{cat}{}^{-1}$ h^{-1}. Electron paramagnetic resonance (EPR) shows electrons are emitted in the solution by the charged FEP, during ultrasonication. EPR and isotope labelling experiments show H_2O_2 is formed from hydroxyl radicals (HO•) or two superoxide radicals ($O_2{}^{\bullet-}$) generated by CEC. Finally, it is traditionally believed such radicals migrate in the solution by Brownian diffusion prior to reactions. However, ab-initio molecular dynamic calculations reveal the radicals can react by exchanging protons and electrons through the hydrogen bonds network of water, i.e., owing to the Grotthuss mechanism. This mechanism can be relevant to other systems, artificial or natural, generating H_2O_2 from air and water.

1. Introduction

Hydrogen peroxide (H_2O_2) is well recognized by the general public as an antiseptic and bleaching agent.[1] However, its importance to the industrial sector, and as a potential energy carrier, is lesser-known outside of industrial and scientific communities.[1] Despite H_2O_2's reputation as a green oxidant, it is only as environmentally friendly as the production and supply chains behind it. Consequently, as the demand for H_2O_2 grows,[2] it is crucial we develop alternative processes to the currently employed anthraquinone oxidation/reduction process.[3] Indeed, this method requires large-scale centralized facilities in order to maintain the costs of operation at acceptable levels,[3b] and the use of hydrogen gas, mainly sourced from light hydrocarbons precursors.[3b,4] To address this issue, many research efforts focus on developing electrochemical routes toward an on-demand, decentralized and low-cost production of H_2O_2.[3b,5] Some electrochemical reactions can even be conducted in ambient conditions and produce H_2O_2 from air and water.[3b,6] This can also be achieved using photocatalysts,[7] and piezo-catalysts,[8] for in situ hydrogen H_2O_2 generation. However, achieving record efficiencies often requires complex and/or expensive designs, or the use of sacrificial agents.[7,8] In contrast, we herein propose to employ a different method generating H_2O_2 from air and water by contact-electro-catalysis. This mechanism allowed us to

A. Berbille, X.-F. Li, Y. Su, X. Zhao, L. Zhu, Z. L. Wang
CAS Center for Excellence in Nanoscience
Beijing Institute of Nanoenergy and Nanosystems
Chinese Academy of Sciences
Beijing 101400, China
E-mail: zhulaipan@binn.cas.cn; zlwang@gatech.edu
A. Berbille, Y. Su, L. Zhu, Z. L. Wang
School of Nanoscience and Engineering
University of Chinese Academy of Sciences
Beijing 100049, China
X.-F. Li
China Key Laboratory of Advanced Materials (MOE)
School of Materials Science and Engineering
Tsinghua University
Beijing 100084, China
S. Li
School of Advanced Materials
Shenzhen Graduate School
Peking University
Shenzhen 518055, China
Z. L. Wang
School of Materials Science and Engineering
Georgia Institute of Technology
Atlanta, GA 30332-0245, USA
Z. L. Wang
Yonsei Frontier Lab
Yonsei University
Seoul 03722, Republic of Korea

The ORCID identification number(s) for the author(s) of this article can be found under https://doi.org/10.1002/adma.202304387

DOI: 10.1002/adma.202304387

employ commercially available fluorinated ethylene propylene (FEP) to generate 58.87 mmol L^{-1} g_{cat}^{-1} h^{-1} of H_2O_2 in deionized (DI) water, using ultrasound driven contact-electrification. This result surpasses recently published piezo-catalysts.

Introduced in 2022, contact-electro-catalysis (CEC) is an emerging catalytic principle that exploits the exchange of charges during contact-electrification at the interface of water and a solid to initiate or accelerate chemical reactions.[9] While it was thought previously that contact-electrification at water-solid interfaces results mostly from transfers of ionic species, recent works demonstrated that, in some cases, electron transfers were dominating.[10] This is notably the case for fluorinated polymers,[11] and highly hydrophobic ceramics.[12] This property endowed fluorinated polymers with the best activity in CEC degradation of azo dyes.[9] It has been proposed electron transfers during contact-electrification occurs, when atoms or molecules of a pair of materials collide, owing to the overlap of their electron-clouds.[13] And, triboelectric electron transfers are now considered a possible initial step in the formation of the electrical-double layer (EDL), and to be foundational to the working principle of solid-liquid triboelectric nanogenerators.[10b,14] The first reports of contact-electro-catalysis employed ultrasonication to trigger the mechanism, by generating high frequency contact-electrification cycles at the interfaces of polymer powders or treated films.[9,15] In these publications, it was consistently found CEC produces hydroxyl ($HO^{\bullet}$), superoxide ($O_2^{\bullet-}$) and hydroperoxyl ($HO_2^{\bullet}$) free radicals. One could describe CEC as a mechanism that endows a triboelectric material with the ability to act like a single-electrode electro-catalysis upon contact-electrification at solid-liquid interface, conducting both water oxidation (WOR) and oxygen reduction (ORR) reactions on a single material. Recently, Song et al. verified droplets sliding on a fluorinated polymer slope are capable of producing $HO^{\bullet}$ by contact-electrification, and that $O_2^{\bullet-}$ is produced by excitation of the electrons capture by polytetrafluoroethylene (PTFE) .[16] Moreover, in other works, Zare's group showed that contact-electrification at water-solid interface can lead to, or is involved into, the spontaneous formation of H_2O_2 when water flows in a microfluidic channel or when water microdroplets condensate on various surfaces, owing to exchange of hydroxyl functional groups present at the surface of SiO_2.[17]

In the present publication, we used ultrasound driven CEC at water-polymer interface to produce H_2O_2. The amount of H_2O_2 produced was evaluated by a potassium iodide (KI) method, relying on UV–vis spectrometry (UV–vis).[18] To confirm the coloration observed resulted from a reaction with H_2O_2, we employed a quantitative nuclear magnetic resonance (NMR) detection method.[19] The state of the catalyst before and after the reaction was characterized by X-ray photoelectron spectroscopy (XPS) and scanning electron microscopy (SEM). We propose that, after the generation of radicals by contact-electrification, H_2O_2 is formed through Grotthuss mechanism.[20] To test this hypothesis, we conducted experiments using ^{18}O labeled water and oxygen, whose results were evaluated by liquid chromatography mass spectroscopy (LC-MS).[20d] And, we employed ab initio molecular dynamic (AIMD) simulation to verify our Grotthuss-based hypothesis. This work introduces an alternative path towards H_2O_2 evolution from ordinary air and pure water, not requiring the use of complex catalysts designs or sacrificial agents. We also aim at deepening our knowledge of the physicochemical processes surrounding liquid-solid contact-electrification, and CEC.

2. Results

2.1. Ultrasonication of Water in Presence of Air and Fluorinated Polymers Produces Hydrogen Peroxide

When we ultrasonicate DI water (50 mL at 40 kHz, 110 W) in presence of fluorinated ethylene propylene (FEP) microparticles (5 to 30 mg), we observe the production of H_2O_2. Knowing the systems only comprises water, FEP, and air, we propose the evolution of H_2O_2 originates from the oxidation of water and reduction of oxygen by contact-electro-catalysis at water-FEP interface (**Figure 1**a). To evaluate the evolution of hydrogen peroxide during the experiment we relied on a previously reported potassium iodide (KI) method that employs ammonium molybdate as a catalyst.[18] More details are available in the Methods section. In fully optimized conditions, (50 mL, 5 mg of FEP, at 20 °C), the kinetic rate of H_2O_2 evolution from air and water reaches 58.87 mmol L^{-1} g_{cat}^{-1} h^{-1} (Figure 1b; Figure S1, Supporting Information). The kinetic rate is higher than most recently reported piezo-catalytic experiment conducted in comparable conditions.[8,21]

As depicted in Figure 1c, ultrasonicating the solution in absence of catalysts still leads to a slight increase in the concentration of H_2O_2. However, the concentration does not exceed 0.017 mmol L^{-1}, after 1 h. Meanwhile, in presence of 10 mg FEP, we obtained 0.391 mmol L^{-1} in the same period. This slight increase in absence of catalyst can be attributed to the dissociation of water by ultrasonic cavitation. To ensure visible light irradiations are not influencing the outcome of the reaction, a control experiment in dark conditions has been conducted, showing illumination does not promote or hinders H_2O_2 evolution in our experiment (see Figure S2, Supporting Information). We also considered that particles can act as a source of physical defects in the medium, thus enhancing the generation of cavitation bubbles by ultrasounds. To evaluate the potential contribution of this effect, we have introduced an equivalent amount of high-density polyethylene (HDPE) micro-powder. HDPE was chosen as a control material owing to its extremely poor contact-electrification ability, resulting in a quasi-null contact-electro-catalytic activity.[9,11,15b] In this experiment, we obtained similar results to what was obtained in absence of catalyst. Therefore, we consider the contribution of dissociation by ultrasonic cavitation to the evolution of H_2O_2 is not significant, here. To ensure the observations made by UV–vis resulted from the generation of H_2O_2, we attempted the detection of H_2O_2 by NMR spectroscopy.[19] The parameters and protocols for this experiment are reported in the Methods section. In Figure 1d, the upper part shows the signal of H_2O_2 obtained by NMR from a standard sample diluted down to 0.005% of concentration. NMR spectra for other standard samples, at various concentrations, are reported in Figure S3 (Supporting Information). The lower part shows the result obtained from the ultrasonication of water in presence of FEP after 5 min. The position of both peaks, at 10.94 ppm, are matching perfectly, confirming that we have indeed produced H_2O_2 during the experiment.

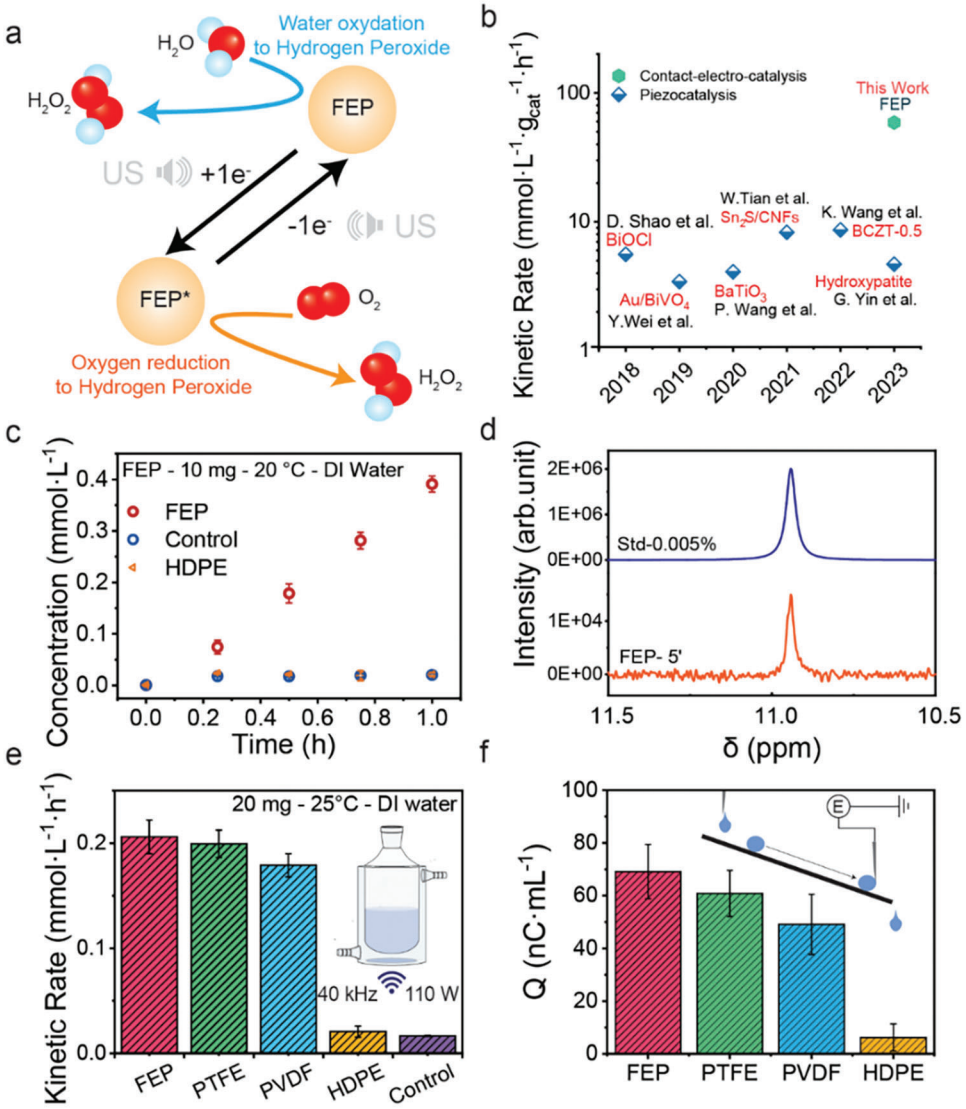

Figure 1. Ultrasonication of water in presence of fluorinated microplastics produces H_2O_2. a) Schematic illustration of generating H_2O_2 from water and oxygen by ultrasonication (US) in presence of FEP. b) Chart comparing the kinetic rate of recently reported piezo-catalysis[8,21] experiments for the production of air and water to the present work in fully optimized conditions. c) Study of H_2O_2 evolution during ultrasonication in presence of FEP micro powder (10 mg), HDPE micro powder (10 mg) and in absence of catalysts (control). d) Quantitative detection of H_2O_2 by NMR spectroscopy, including a standard sample at 0.005% (std-0.005%) (Top) and a sample after 5 min of ultrasonication in presence of FEP (Bottom). e) Kinetic rate of H_2O_2 production for various materials (FEP, PTFE, PVDF, HDPE) and for a control (ultrasonication of water without a catalyst). f) Charges exchanged by a droplet of water (34 µL) sliding on slopes made of the same materials as the ones used in the CEC experiment. The illustration of the setup for the droplet experiment is inserted in the graph. All errors bars are obtained from 3 reproduced experiments.

We also reproduced the H_2O_2 evolution experiment for various dielectric polymer particles (Figure 1e), namely FEP, polytetrafluoroethylene (PTFE), polyvinylidene fluoride (PVDF), and HDPE, revealing the kinetic rate is decreasing in that order. In order to verify the mechanism involved is contact-electro-catalysis, and determine which material is the best catalyst, we compared the trend observed in the chemical experiment with the discrepancy in terms of contact-electrification ability between the same materials (Figure 1f). If contact-electro-catalysis is involved in this process, we should observe a correlation between the catalytic activity and contact-electrification ability of the materials tested, and a superior charge withdrawing ability from FEP in particular. The values of droplets' charge density were obtained through a sliding droplet experiment (see inset of Figure 1f and details in Experimental Section).[22] We observed the catalytic activity towards H_2O_2 evolution and the density of charges exchanged during the sliding droplet experiment follow the same trend. FEP stands out as the best contact-electro-catalyst toward H_2O_2 evolution owing to its superior contact-electrification ability with water. Therefore, we employed FEP for the rest of the experiments. The superior ability of FEP to withdraw electrons from water is attributed to the presence of -F and -CF_3 functional groups, owing to their high electron-withdrawing properties.[9,11,12] The powder was characterized before and after ultrasonication, by SEM (Figures S4,S5,

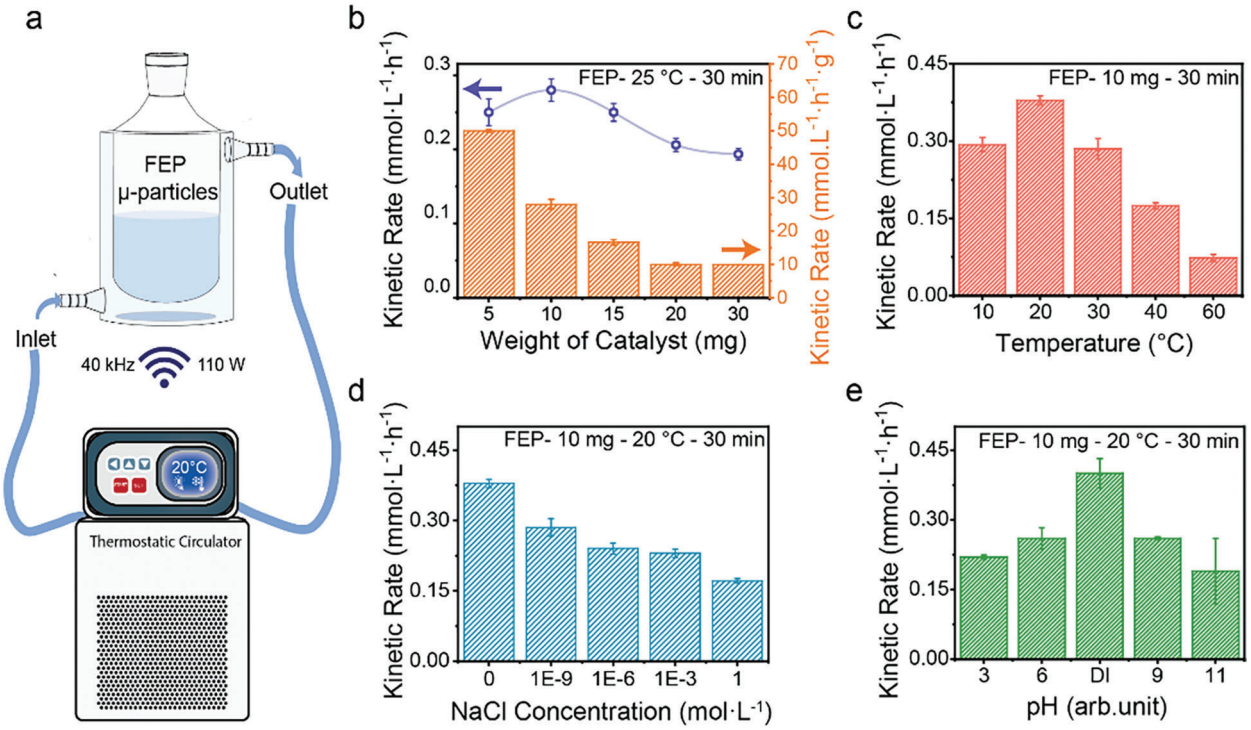

Figure 2. Optimization of the reaction conditions. a) Illustration of the experimental setup comprising a thermostatic circulator that regulates the temperature of the reactor, and an ultrasonic bath (40 kHz, 110 W). b) Kinetic rate of H_2O_2 generation according to the mass of FEP added in a 50 mL solution of DI water, at 25 °C. c) Influence of temperature on the kinetic rate of the generation of H_2O_2. d) Influence of the salt concentration (NaCl) on the kinetic rate of H_2O_2 formation. e) Influence of the pH on the kinetic rate of the production of H_2O_2. The error bars represent one standard deviation using 3 replicate measurements.

Supporting Information) and XPS (Figure S6–S13, Supporting Information). It appears that no significant changes in terms of morphology or composition occurred during the experiment, in good agreement with previously reported results.[9] An illustration of the setup employed for all the catalysis experiments is presented in **Figure 2**a.

In the result reported in Figure 1b, when the conditions are optimized to reach the best yield per gram of catalyst, for 50 mL of solution, we have utilized the following parameters: FEP, 5 mg, 20 °C, in DI water (Figure S1, Supporting Information). To determine these conditions as optimal, we first needed to explore parameters of influence, one by one, starting with the mass of catalyst, FEP here (Figure 2b). The results show the absolute kinetic rate only slightly changes by increasing or decreasing the catalyst to DI water mass ratio. This can be explained by the fact that most of the hydrophobic powder is floating, forming a film at the surface, rather than being dispersed in the solution. Kinetic rate is the highest when introducing 10 mg of FEP, making this amount of catalyst more appropriate for observations. However, it is worth mentioning that if we consider the results per weight of catalyst, then using 5 mg is economically more efficient. Indeed, the yield of H_2O_2 per gram of catalyst increases drastically compared to the experiments at 10 mg. In Figure 2c, we report the results of an experiment evaluating the effect of temperature on H_2O_2 evolution. We observe, first, an increase in the kinetic rate from 10 °C to 20 °C, which could be explained by more favorable thermodynamic conditions and an improved electron transfer. However, when we cross the 20 °C mark to 30 °C and upward, the kinetic rate of the reaction decreases sharply. We also observed this phenomenon in a previous experiment, and found that FEP microparticles have a glass transition temperature of ≈35 °C.[15a] As a result, the polymer is less capable of extracting electrons from water upon impact as temperature increases. Therefore, the temperature was maintained at 20 °C for the rest of the experiments. The effect of salt concentration and pH on charge exchanges at water-solid interfaces during contact-electrification has been extensively reported.[10,12b] According to these experiments, if the production of H_2O_2 during ultrasonication in presence of FEP is actually resulting from contact-electrification at solid-water interface, we should observe a decrease in the kinetic rate as salt concentration increases or as pH deviates from that of DI water. In Figure 2d, we observe that the salt concentration affects the kinetic rate of the reaction greatly, decreasing as NaCl concentration increases. The same observation can be made for the effect of pH, as reported in Figure 2e, with a decrease in the kinetic rate of H_2O_2 evolution as pH tends toward 1 or 14 alike. In conclusion, the optimal conditions for the production of H_2O_2 by CEC at FEP/Water interface are: 0.1 g of catalyst per liter of DI water, at a temperature of 20°C.

2.2. Production of Radicals by Ultrasonically Driven Contact-Electrification

Our working hypothesis, concerning the generation of H_2O_2 is based on the first steps being an ultrasonically induced

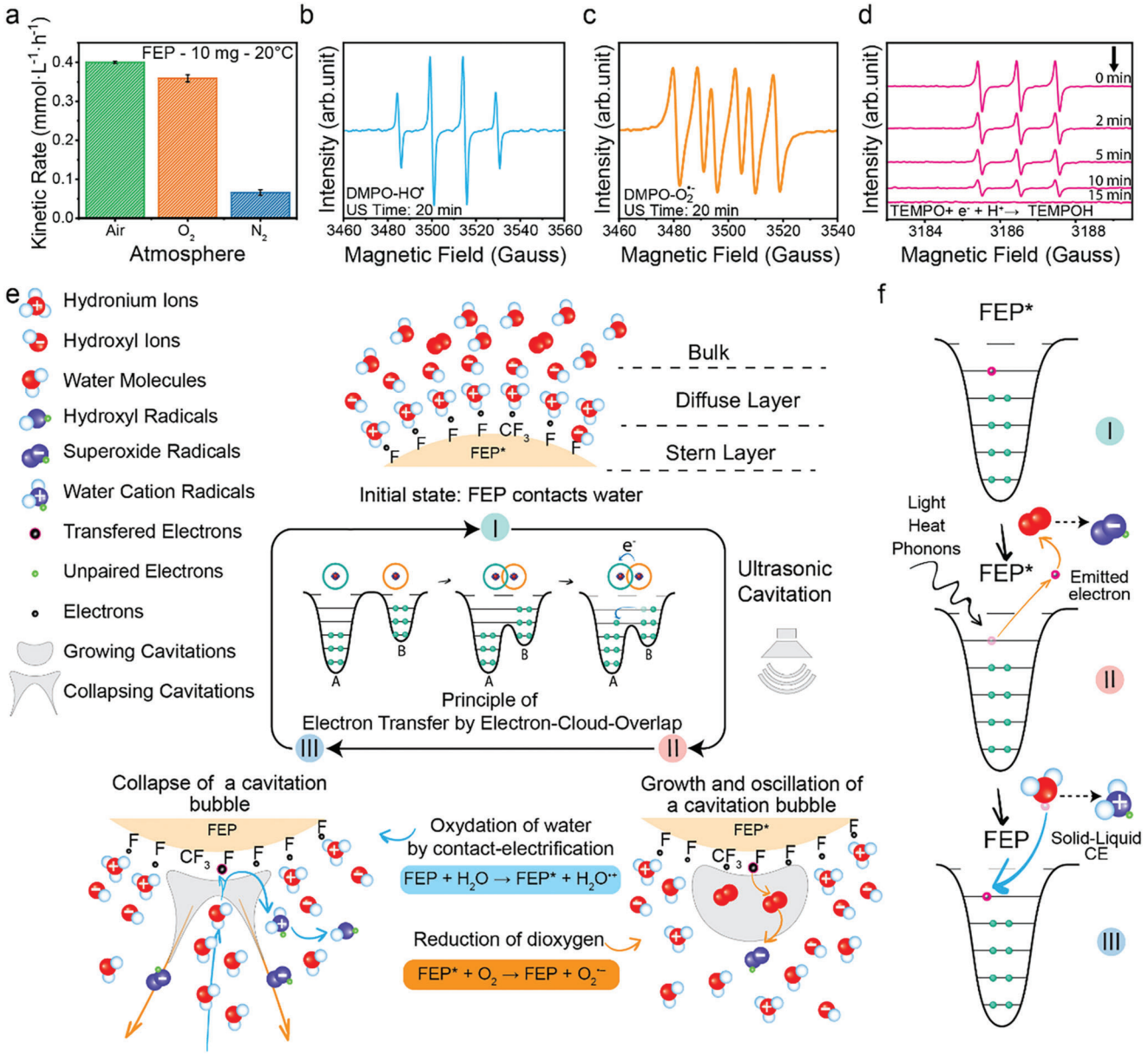

Figure 3. Mechanism for the generation of hydroxyl radicals and superoxide radicals by contact electro-catalysis. a) Effect of the nature of the gas on H_2O_2 evolution. Detection by EPR of b) DMPO-HO•, c) DMPO-O_2•-, and d) the loss of signal intensity from TEMPO as it is reduced to TEMPOH by addition of 1 electron and 1 proton during CEC. e) Illustration of the proposed general principle of the mechanism of radicals' generation by ultrasound induced CEC in aqueous solution. f) Illustration of the proposed mechanism behind the exchange of electrons at step I, II, and III of the contact-electro-catalytic process. All errors bars are obtained from 3 reproduced experiments.

high-frequency exchange of electrons between water and a solid by contact-electrification, followed by the capture of the induced electrons by dioxygen. First, we verified the role of dioxygen in the process by measuring the kinetic rate of H_2O_2 production when the solution is saturated with N_2 or O_2. When the solution is saturated with O_2, we see the H_2O_2 yield per hour decreases slightly. This could be explained by the previously reported detrimental effect of oxidative atmospheres on contact-electrification.[23] When the saturating gas is replaced by N_2, the kinetic rate of the reaction decreased drastically, confirming the importance of ORR steps in H_2O_2 evolution by CEC. The fact the system still produces H_2O_2 in anaerobic conditions shows that, at least, some of it is produced by CEC driven WOR. To verify the hypothesized production of HO• and O_2•−, we conducted spin trapping experiments, and detected the spin trap adducts through electron paramagnetic resonance (EPR).

In **Figure 3**b, we observe the signal produced by the adducts obtained from the reaction between 5,5-dimethyl-1-pyrroline N-oxide (DMPO) and hydroxyl radicals, namely DMPO-HO•, after 20 min of ultrasonication in presence of FEP.[9] Figure 3c displays the EPR spectrum of the adducts obtained from the reaction of DMPO with O_2•−, DMPO-O_2•−,[24] after 20 min of

ultrasonication in presence of FEP. A negligeable amount of TEMPO adducts is obtained from the reaction of singlet oxygen ($^1O_2$) and 2,2,6,6-Tetramethyl-4-piperidone hydrochloride (TEMP),[25] as seen in Figures S14,S15 (Supporting Information). Finally, EPR measurements also allowed us to detect electrons involved in the reaction, by introducing the stable radical TEMPO in our aqueous solution, and ultrasonicating it for 15 min in presence of FEP.[26] If electrons are emitted by charged FEP in the solution during CEC, the intensity of the signal of TEMPO should decrease. Indeed, the final product of the reaction of TEMPO with 1 electron and 1 hydronium ion, TEMPOH, is non-paramagnetic and therefore not detectable in EPR. In Figure 3d, we observe the signal decreases rapidly, as we ultrasonicate the TEMPO solution in presence of FEP, revealing that the latter is capable of emitting electrons in the solution. Details about the methods to acquire the signals and data treatment are reported in the Experimental Section. The raw and smoothed spectra acquired at 0, 5, 10, 20, and 30 min for the detection of hydroxyl, and superoxide radicals, and singlet oxygen, by EPR, are available in Figures S14–S19 (Supporting Information). We propose to describe the mechanism of CEC as follows (Figure 3e). At first, when the triboelectric powder touches the water, it obtains electrons from the liquid by solid-liquid contact-electrification (SL-CE). During this event, a small amount of water is oxidized to water radical cations ($H_2O^{\bullet+}$), leading to the formation of $HO^\bullet$ (Equations (1) and (2)), and FEP gets charged negatively, noted FEP* (Figure 3e, I and Figure 3f, I). Electron exchanges during this initial contact-electrification are believed to derive from the overlap of the electron clouds, when two atoms A and B are colliding in the repulsive region,[10b,24] as described in the central inset of Figure 3e. After the initial impact, ions accumulate at the surface of the charged particles to form a static electrical double layer (EDL = Stern Layer + Diffuse Layer) (Figure 3e, I). When the ultrasonication starts, cavitation bubbles form from defects in the bulk of water, such as dissolved gas and particles (Figure 3e, II). The surrounding water and the bubbles generated at the surface or in the vicinity of FEP* can both contain O_2. This dioxygen could capture electrons either by solid-gas contact-electrification (SG-CE) (Equations (3) and (4)), or upon reacting with emitted electrons, amid the input of energy provided by either environmental visible light, or heat and phonons generated by ultrasonic cavitations (Equations (5) and (6)) (Figure 3f, II). Thus, $O_2^{\bullet-}$ are formed. Those radicals can react with hydronium ions to form $HO_2^\bullet$ (Equation (4)).[9] Finally, as the cavitation bubbles violently collapses, the microjet generated projects water molecules on the surface of the now discharged surface of FEP. Water loses one electron to the surface of FEP and forms a $H_2O^{\bullet+}$ (Equation (1)),[27] that decays into $HO^\bullet$ (Equation (2)) (Figure 3e and Figure 3f, III).

$$H_2O_{(l)} + FEP_{(s)} \xrightarrow{SL-CE} H_2O^{\bullet+}_{(aq)} + FEP^*_{(s)} \quad (1)$$

$$H_2O^{\bullet+}_{(aq)} + H_2O_{(l)} \rightarrow H_3O^+_{(aq)} + HO^\bullet_{(aq)} \quad (2)$$

$$O_{2_{(g)}} + FEP^*_{(s)} \xrightarrow{SG-CE} O^{\bullet-}_{2_{(aq)}} + FEP_{(s)} \quad (3)$$

$$O^{\bullet-}_{2_{(aq)}} + H_3O^+_{(aq)} \rightarrow HO^\bullet_{2_{(aq)}} + H_2O_{(l)} \quad (4)$$

$$FEP^*_{(s)} \xrightarrow{\substack{photons,\\ phonons,\\ heat}} e^- + FEP_{(s)} \quad (5)$$

$$O_{2_{(g)}} + e^- \rightarrow O^{\bullet-}_{2_{(aq)}} \quad (6)$$

We should mention the pressure of the microjet increases the probability of an electron transfer by contact-electrification, owing to the dependence of the latter on both pressure and velocity of the molecules.[22b,24]

It is worth noting air contains not only N_2 and O_2 but other gases, including ozone (O_3), that could act as an electron transfer agent. According to literature, alternative paths involving O_3 for the formation of superoxide, hydroxyl and hydroperoxyl radicals from hydroxyl anions, and ultimately H_2O_2, exist.[28] These reaction paths are suppressed when pure O_2 or N_2 is bubbled in the solution, leading to a slightly lower yield even when the solution is saturated with O_2. The equations related to these paths of reaction are reported below (Equations (7–14)).[28]

$$O_{3_{(g)}} + HO^-_{2_{(aq)}} \rightarrow HO^\bullet_{(aq)} + O^{\bullet-}_{2_{(aq)}} + O_{2_{(g)}} \quad (7)$$

$$O_{3_{(aq)}} + HO^-_{(aq)} \rightarrow O^{\bullet-}_{2_{(aq)}} + HO^\bullet_{2_{(aq)}} \quad (8)$$

$$O_{3_{(g)}} + HO^-_{(aq)} \rightarrow HO^-_{2_{(aq)}} + O_{2_{(g)}} \quad (9)$$

$$O_{3_{(g)}} + HO^-_{(aq)} \rightarrow O^{\bullet-}_{3_{(aq)}} + HO^\bullet_{(aq)} \quad (10)$$

$$H_2O_{(l)} + HO^\bullet_{2_{(aq)}} \leftrightarrow H_3O^+_{(aq)} + O^{\bullet-}_{2_{(aq)}} \quad (11)$$

$$O_{3_{(g)}} + O^{\bullet-}_{2_{(aq)}} \rightarrow O^{\bullet-}_{3_{(aq)}} + O_{2_{(g)}} \quad (12)$$

$$O^{\bullet-}_{3_{(aq)}} + H_2O_{(l)} \rightarrow HO^\bullet_{(aq)} + HO^-_{(aq)} + O_{2_{(g)}} \quad (13)$$

$$HO^-_{2_{(aq)}} + H_3O^+_{(aq)} \leftrightarrow H_2O_{2_{(aq)}} + H_2O_{(l)} \quad (14)$$

Moreover, another phenomenon that has not been discussed in the literature treating of contact-electro-catalysis is the ability of the corona of gaseous microbubbles in water to promote electrochemical reaction at the surface of an electrode.[29] Indeed, as reported by Y. B. Vogel et al., the unbalanced accumulation of hydroxyl radicals at the interface of air and water formed by gas microbubbles creates an electrical potential capable of facilitating or triggering the oxidation of hydroxyl anions to hydroxyl radicals (Equation 15).[29a] In this case, the remaining electron could participate in the formation of superoxide radical from dioxygen (Equation 6). Alternatively, FEP could act as a drain for the electrons lost by hydroxyl anions, similarly to what has been observed for microbubbles pinned to the anode (Equation 16).[29]

$$HO^-_{(aq)} \rightarrow HO^\bullet_{(aq)} + e^- \quad (15)$$

$$HO^-_{(aq)} + FEP_{(s)} \rightarrow HO^\bullet_{(aq)} + FEP^*_{(s)} \quad (16)$$

Although we have described how the radicals were generated from water and oxygen, it is important to verify they are the actual sources of atoms for the formation of H_2O_2 by CEC. To that effect, we conducted an ^{18}O isotope labeling experiment (**Figure 4**a–d).

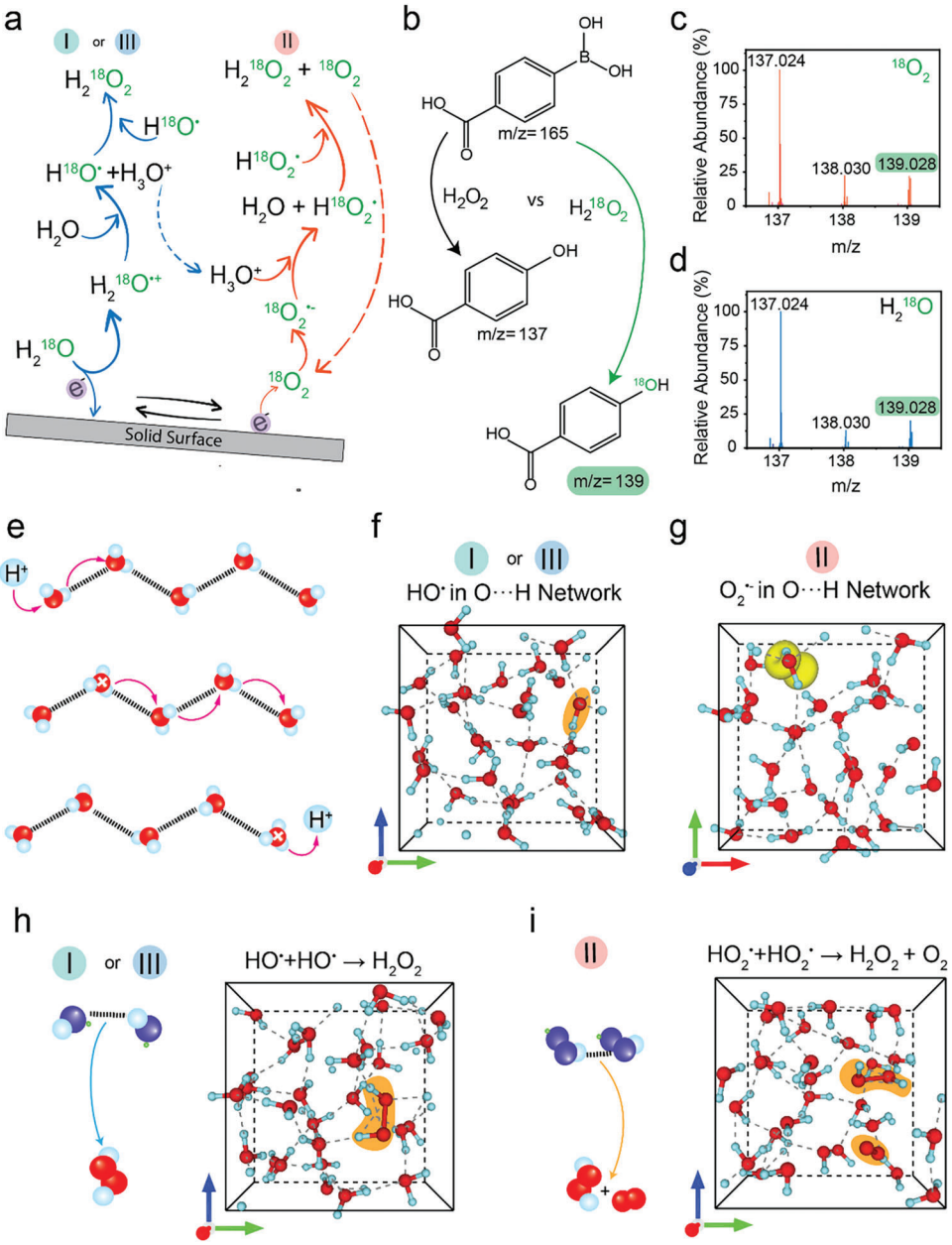

Figure 4. Demonstration of H_2O_2 evolution mechanism from water and air during contact-electro-catalysis by labelling experiments and Ab-Initio Molecular Dynamic calculations. a) Representation of the reaction of 4-carbonxyphenylboronic acid (4-CPB) with unlabeled (black arrow) and labeled (green arrow) H_2O_2. b) Mass spectrum of ^{18}O labeled dioxygen experiment obtained by LC-MS. c) Mass spectrum of ^{18}O labeled water experiment obtained by LC-MS. d) Illustration of proposed reaction path for ^{18}O labeling of H_2O_2, using heavy water or heavy dioxygen. e) Illustration of proton hoping by Grotthuss mechanism in water hydrogen bond network. f–i) Results of the AIMD simulation of the hydrogen bond network, under 30% densification of the aqueous solution, for f) one hydroxyl radical placed in the simulation cell (highlighted in orange), g) one superoxide radical obtained by adding 1 electron in a simulation cell containing O_2 (the magnetic moment of the charged oxygen appears in yellow), h) two hydroxyl radicals placed in the simulation cell react to form H_2O_2 (highlighted in orange), i) two hydroperoxyl radicals placed in the simulation cell react to form H_2O_2 and O_2 (highlighted in orange). Simulation color code: O, red; H, blue. Direction of arrow: *a*, red; *b*, green; *c*, blue.

2.3. Mechanism for the Evolution of H_2O_2 from Air and Water by Contact-Electro-Catalysis Studied through ^{18}O isotope Labeling Experiments and AIMD Simulation

The working hypothesis, presented in Figure 4a, is that after the initial oxidation of water (Equation (17)), two HO• can react to form H_2O_2 (Equation (18)). Meanwhile, the two $HO_2^{\bullet}$ produced by reduction of dioxygen (Equation (19)) react to form H_2O_2 (Equation (20)).

$$2H_2O_{(l)} + FEP_{(s)} \xrightarrow{SL-CE} HO^{\bullet}_{(aq)} + FEP^{*}_{(s)} + H_3O^{+}_{(aq)} \quad (17)$$

$$2HO^{\bullet}_{(aq)} \rightarrow H_2O_{2(aq)} \quad (18)$$

$$O_{2(aq)} + FEP^{*}_{(s)} + H_3O^{+}_{(aq)} \xrightarrow{SG-CE\ or\ photons,\ phonons,\ heat} HO^{\bullet}_{2(aq)} + H_2O_{(l)} + FEP_{(s)} \quad (19)$$

$$2HO^{\bullet}_{2(aq)} \rightarrow H_2O_{2(aq)} + O_{2(g)} \quad (20)$$

To verify the proposed mechanism, we used labeling experiments. In one case we replaced 20% of the volume of water by $H_2{}^{18}O$. If the oxidation of labeled water by contact-electrification produces $HO^{\bullet}$ that participates in H_2O_2 evolution, we should obtain isotope labeled $H_2{}^{18}O_2$ at the end of the experiment (Figure 4a, left). In another experiment we bubbled the solution with $^{18}O_2$ for 10 min at 20 mL min^{-1}, expecting to obtain $H_2{}^{18}O_2$, similarly (Figure 4a, right). The samples obtained after both experiments are then mixed with a solution of 4-carboxyphenylboronic acid (4-CPB, $C_7H_7BO_4$), as described in Figure 4b and the Experimental section. The deborylation reaction that ensue marks the product of the reaction with ^{18}OH groups if the H_2O_2 is produced from labeled water or oxygen. The labeled product, $C_7H_6O_2{}^{18}O$, can be identified by LC-MS, characterized by a difference of charge to mass ratio (m/z) of +2 (Figure 4b) with the unlabeled product $C_7H_6O_3$. The LC-MS displayed in Figure 4c shows the reduction of $^{18}O_2$, by emitted electron or by SG-CE, actually leads to the production of $H_2{}^{18}O_2$. Similarly, the LC-MS results of the experiment employing labeled water (Figure 4d) shows that oxidation of labeled water by CEC yields $H_2{}^{18}O_2$. The total ion chromatograms and extracted ion spectra of these experiments are available in Figures S20–S23 (Supporting Information). We therefore confirmed that H_2O_2, is actually produced by CEC triggered WOR and ORR. However, it does not explain how the proton and electron exchanges, leading to the formation of H_2O_2 from the $HO^{\bullet}$ and $HO_2{}^{\bullet}$, happen in the bulk of water. We propose they could be occurring by proton shuttling through the hydrogen bond network, i.e., owing to the Grotthuss mechanism (Figure 4e).[20] To explore this hypothesis, we employed AIMD simulation, using 34 water molecules in a cubic simulation cell. The results presented in Figure 4f–i are calculated at a 30% densification to take into account the pressure generated microjet during cavitation collapse (see Note S1, Supporting Information).[30] In these conditions, the results of the calculation presented in Figure 4f,g show both $HO^{\bullet}$ and $O_2{}^{\bullet-}$ could exist in the hydrogen bond network, giving them a chance to react. $O_2{}^{\bullet-}$ is obtained by adding one electron in the system, corresponding the electron emitted in Figure 3e, II and Figure 3f, II. The calculation shows the electron spontaneously reacts with the dioxygen suggesting water cannot compete with O_2 for electrons, in good agreement with the mechanisms presented in Figure 3e,f and Figure 4a. While the $O_2{}^{\bullet-}$ could also exist in atmospheric pressure conditions, it is important to mention it is not the case for a lonely $HO^{\bullet}$ (Figure S24a, Supporting Information). It seems then, for CEC-WOR path, the pressure generated by the microjet during the cavitation collapse not only helps with the electron transfer between water and FEP,[9,22b] but also stabilizes $HO^{\bullet}$ radicals in the hydrogen bound network, giving them better chances to react before decaying.

As shown in the results presented in Figure 4h, we observed that if two $HO^{\bullet}$ are placed in water's hydrogen bonds network, they react and form H_2O_2. This mechanism is also verified under atmospheric pressure condition (Figures S24,S25, Supporting Information). Our description of CEC-ORR path towards H_2O_2 evolution, presented in Figure 4a, states that two $HO_2{}^{\bullet}$ react to form H_2O_2 and O_2. Once again, we ran our calculation after introducing two $HO_2{}^{\bullet}$ in the hydrogen bond network. The final result shows H_2O_2 and O_2 (Figure 4i) are formed, in good agreement with previously formulated hypotheses. While this mechanism is able to generate H_2O_2 at atmospheric pressure as well, it is not verified under 50% densification, contrary to the case of $HO^{\bullet}$ (Figure S25, Supporting Information).

3. Conclusion

We have shown that microplastics endowed with high solid-liquid contact-electrification (SL-CE) ability, such as FEP, are able to produce a high amount of H_2O_2 through ORR and WOR by contact-electro-catalysis. The kinetic rate obtained for each polymer is correlated with their contact-electrification ability. During CEC, oxidation of water by SL-CE leads to the formation of $HO^{\bullet}$ radicals. The then charged polymer appears to be able to reduce dissolved O_2. We propose O_2 is either reduced by SG-CE, upon collapse of cavitation bubbles, or by electrons ejected from FEP* due to excitation from visible light or phonons and heat generated by ultrasonic cavitation. The overall equations for CEC driven WOR (Equation (21)) and CEC driven ORR (Equation (22)) generating H_2O_2 by CEC can be written as:

$$4H_2O_{(l)} + 2FEP_{(s)} \xrightarrow{SL-CE} H_2O_{2(aq)} + 2FEP^{*}_{(s)} + 2H_3O^{+}_{(aq)} \quad (21)$$

$$O_{2(g)} + 2FEP^{*}_{(s)} + 2H_3O^{+}_{(aq)} \xrightarrow{SG-CE\ or\ photons,\ phonons,\ heat} H_2O_{2(aq)} + 2H_2O_{(l)} + 2FEP_{(s)} \quad (22)$$

We found the optimized parameters to observe the reaction, for a volume of water of 50 mL are 10 mg of FEP, at 20 °C. In these conditions, the reaction is able to produce 0.391 mmol L^{-1} h^{-1}. However, one should note it is more economically efficient to decrease the weight of catalyst by half (5 mg). By doing so, the yield per gram of catalyst is 56% higher. We studied the mechanism behind the formation of H_2O_2 employing EPR, and an isotope labelling experiment. It shows that, indeed, H_2O_2 formation by CEC originates from water and dissolved dioxygen in water. The mechanism of contact-electro-catalysis could be described as a single-electrode electrochemical process, performing ORR and WOR on a single particle, that is initially triggered by liquid-solid contact-electrification. We finally proposed that the process by which 2 $HO^{\bullet}$ or 2 $HO_2{}^{\bullet}$ radicals react to form H_2O_2 could be partially explained by proton-shuttling through Grotthuss mechanism. The results of the AIMD simulation are in good agreement with the formulated hypothesis. The mechanism proposed,

here, should be applicable to other systems, natural or artificial, to explain how radicals formed during WOR and ORR can generate H_2O_2 in the bulk of water. We would also like to mention experimental studies about contact-electrification at solid-liquid interfaces consistently show liquids capable of forming hydrogen bonds networks are better at exchanging charges with the solid substrate.[22] This could be the result of rapid charge recombinations in the bulk of the liquid, owing to the Grotthuss mechanism. This mechanism is extremely rapid in water, happening in burst as stated by Konermann and Kim,[20b] thus it could explain why water outperforms all other liquids in SL-CE. Further experimental and theoretical studies should be conducted to confirm the proposed role of Grotthuss mechanism in SL-CE. Concerning the future development of CEC, researchers should continue to explore the potential ability of CEC to perform other organic and inorganic reactions. Understanding the mechanism deeper can help us finding original paths to harness its power for blue energy harvesting and contact-electro-catalysis. With regards to the present use of catalysts containing polyfluoroalkyl substances (PFAS), and the resulting environmental pollutions, we should concentrate efforts on making new contact-electro-catalytic materials. They could be made of ceramics or modified polymers that shall be designed to be better performers while reducing the environmental impact. Thus, CEC could become a viable option for delocalized H_2O_2 production.

4. Experimental Section

Reagents: All the reagents were purchased either from Sigma–Aldrich, Macklin or Dojindo.

Spectrophotometric Quantitative Measurement of H_2O_2 Concentration by KI Method: In presence of H_2O_2 in the solution, iodide ions form I_2 (Equation (23)) molecules then in turn form I_3^- (Equation (24)). Ammonium molybdate was used as a catalyst of the reaction between H_2O_2 and I^-, as previously reported.[18]

$$H_2O_{2(aq)} + 2I^-_{(aq)} + 2H_3O^+_{(aq)} \xrightarrow{Mo(VI)} I_{2(aq)} + 4H_2O_{(l)} \quad (23)$$

$$I_{2(aq)} + I^-_{(aq)} \rightarrow I^-_{3(aq)} \quad (24)$$

A fresh titration solution containing KI (48 mmol L^{-1})and ammonium molybdate tetrahydrate ($H_{24}Mo_7N_6O_{24}{\cdot}4H_2O$) (700 µmol L^{-1}) was prepared every week, according to needs. pH was adjusted to 4.

The aliquot (150 µL) was mixed with the titration solution (150 µL) in a sampling tube. After 30 s, the mixture was diluted 5 times in DI water in order to avoid saturation of the signal of the UV–Vis spectrometer. A calibration curve was made, using peaks at 287.0 nm and 350.0 nm, at the beginning of every experiment in order to ensure the titration solution was still working appropriately, using samples of 1, 0.5, 0.25, 0.125, 0.0625 and 0 mM. An example of a calibration curve was reported in Figures S26,S27 (Supporting Information).

Quantitative Detection of H_2O_2 Concentration by NMR: The samples for NMR detection of H_2O_2 were prepared by mixing the aliquot (540 µL) with a solution of 2-(N-Morpholino) ethanesulfonic acid (MES) (60 µL, 1 mmol L^{-1}) in D_2O directly in an NMR tube. The pH was then adjusted using an NMR glass probe (Apera Instrument, Labsen pH electrode) at pH 6.06±0.05, using NaOH and HCl solutions (50 mmol L^{-1}). For the measurement, the temperature was controlled using a cryogenic probe, set at 2 °C, a Gaussian pulse set at 3 ms, and 30 720 scans in 30 min.[19] The measurements were conducted on a Bruker Avance III 700 MHz NMR spectrometer.

Measurement of Charges Exchange Between a Droplet of Water and Various Materials: The material of interest was stuck on a piece of poly(methyl methacrylate), using a layer of adhesive. The thus obtained slope was then placed on a platform with an angle of 55°, relative to the ground. A droplet (34 µL) then hits the slope from a height of 45 mm, and slides on the slope, on a length of 65 mm, before meeting a grounded needle that collects the charges accumulated in the droplet. The signal was acquired through a Keithley 6517B electrometer.

EPR Measurement of Free Radicals: All measurements were obtained using 1024 data points on a Bruker EPR spectrometer.

Measurement of DMPO-HO•: FEP (10 mg) was added in an aqueous solution containing DMPO (5 mL, 100 mmol L^{-1}). The solution was then ultrasonicated for 30 min. Aliquots were sampled and measured at 0, 5, 10, 20, 30 min.

Measurement of DMPO-$O_2^{\bullet-}$: FEP (10 mg) was added in a solution containing DMPO (5 mL, 100 mmol L^{-1}), the solvent in this case consists in a mixture of water and ethanol (9:1 water/ethanol ratio). The solution was then ultrasonicated and aliquots were sampled and measured at 0, 5, 10, 20, 30 min.

Measurement of TEMPO →TEMPOH: FEP (10 mg) was added in a solution containing TEMPO (5 mL, 100 mmol L^{-1}), and the solution was ultrasonicated for 20 min. Aliquots were sampled and measured at 0, 5, 10, 20 min.

O Isotope Labeled Water and Dioxygen Experiment: The negative polarity LC-MS measurements were conducted by first separating the components of the solution using a Waters BEH C18 chromatography column (2.1 × 100 mm, 1.7 µm). Mobile phase A consists in a 0.1% formic acid aqueous solution, while mobile phase B was acetonitrile. Aliquot of 5 µL was injected in the column, set at 40 °C. The column was connected to an Orbitrap Quadrupole-Electrostatic Field Orbitrap High Resolution Tandem Mass Spectrometer (Thermofisher Exactive, USA). Spray voltage was set at 3.5 kV.

^{18}O isotope labeled water experiment: A solution (10 mL) of $H_2{}^{18}O$ (20% V in DI water) was prepared. FEP (2 mg) was then added to the solution and the system was ultrasonicated for 30 min. Aliquot of 1 mL from the final solution was mixed with 1 mL of a 4-carboxyphenylboronic acid (4-CPB, $C_7H_7BO_4$) solution (100 µmol L^{-1}) prepared separately. The product of the deborylation of 4-CPB were then analyzed through LC-MS.

$^{18}O_2$ isotope labeled water experiment: Water of 10 mL with 2 mg of FEP were bubbled with $^{18}O_2$ for 10 min at 20 mL min^{-1}. The description of the rest of the experiment was identical of that for $H_2{}^{18}O$.

AIMD Simulation for Grotthuss Mechanism: In this study, the density functional theory calculations were conducted using the projector-augmented-wave method as implemented in the Vienna ab initio Simulation Pack (VASP) code.[31] The kinetic energy cutoff was set to 450 eV. A conjugate gradient method was applied for geometry optimization, with a Gaussian smearing width of 0.05 eV. The total energy criterion in the electronic self-consistency loop and the force criteria in the ionic relaxation loop was set to 10^{-5} eV and 0.02 eV $Å^{-1}$, respectively. Supercells with 34 molecules of water were used, in combination with a Γ-centered 2 × 2 × 2 k-mesh. The temperature of the AIMD simulations was controlled by the Nose-thermostat, with a target temperature of 300 K and a relaxation time of 1 ps. Empirical Grimme's D3 scheme was employed to take into account the van-der-Waals interactions.

Supporting Information

Supporting Information is available from the Wiley Online Library or from the author.

Acknowledgements

This research was supported by the National Natural Science Foundation of China (grant no.52192613), and sponsored by the CAS-TWAS President's Fellowship (A.B). The author thank the mass spectrometry facility of National Center for Protein Sciences at Peking University for assistance

with the NMR spectroscopy and Dr. Hongwei Li (Peking University, China) for helping with the NMR detection of H_2O_2. The authors would also like to thank Tayeb Kakeshpour (National Institute of Health, USA), for answering our questions about the detection of H_2O_2 by NMR spectroscopy.

Conflict of Interest

The authors declare no conflict of interest.

Author Contributions

A.B. and X.L. contributed equally to this work. A.B. conceived the idea. Z.W., L.Z. supervised the experiments and funded the project. A.B. developed the experimental setups. A.B., Y.S., and X.Z. collected the experimental data. A.B. conducted the formal analysis of experimental results. A.B., X.L., and S.L. discussed the theoretical model. X. L. developed the simulation and collected the simulation data. A.B., and X.L. conducted the formal analysis of the theoretical results. A.B., X.L. prepared the original manuscript. A.B., X.L., Y.S., S.L., X.Z., L.Z., and Z.W. reviewed and edited the manuscript.

Data Availability Statement

The data that support the findings of this study are available from the corresponding author upon reasonable request.

Keywords

contact-electrification, heterogeneous catalysis, hydrogen peroxide, polymers, triboelectrification

Received: May 10, 2023
Revised: June 17, 2023
Published online: October 15, 2023

[1] C. E. Housecroft, A. G. Sharpe, *Inorganic Chemistry*, Pearson Education, London, **2008**.
[2] Hydrogen Peroxide Market Global Forecast to 2027, MarketsAndMarkets, **2023**.
[3] a) J. Fierro, J. M. Campos-martin, G. Blanco-brieva, *Angew. Chem. Int. Ed. Engl.* **2006**, *45*, 6962; b) S. C. Perry, D. Pangotra, L. Vieira, L.-I. Csepei, V. Sieber, L. Wang, C. Ponce de León, F. C. Walsh, *Nat. Rev. Chem.* **2019**, *3*, 442.
[4] a) T. Nishimi, T. Kamachi, K. Kato, T. Kato, K. Yoshizawa, *Eur. J. Org. Chem.* **2011**, *2011*, 4113; b) P. J. Megía, A. J. Vizcaíno, J. A. Calles, A. Carrero, *Energy Fuels* **2021**, *35*, 16403.
[5] a) Z. Lu, G. Chen, S. Siahrostami, Z. Chen, K. Liu, J. Xie, L. Liao, T. Wu, D. Lin, Y. Liu, T. F. Jaramillo, J. K. Nørskov, Y. Cui, *Nat. Catal.* **2018**, *1*, 156; b) C. Xia, S. Back, S. Ringe, K. Jiang, F. Chen, X. Sun, S. Siahrostami, K. Chan, H. Wang, *Nat. Catal.* **2020**, *3*, 125; c) H. W. Kim, M. B. Ross, N. Kornienko, L. Zhang, J. Guo, P. Yang, B. D. McCloskey, *Nat. Catal.* **2018**, *1*, 282.
[6] X. Zhang, Y. Xia, C. Xia, H. Wang, *Trends Chem.* **2020**, *2*, 942.
[7] Y. Ju, H. Li, Z. Wang, H. Liu, S. Huo, S. Jiang, S. Duan, Y. Yao, X. Lu, F. Chen, *Chem. Eng. J.* **2022**, *430*, 133168.
[8] K. Wang, M. Zhang, D. Li, L. Liu, Z. Shao, X. Li, H. Arandiyan, S. Liu, *Nano Energy* **2022**, *98*, 107251.
[9] Z. Wang, A. Berbille, Y. Feng, S. Li, L. Zhu, W. Tang, Z. L. Wang, *Nat. Commun.* **2022**, *13*, 130.
[10] a) Z. Tang, S. Lin, Z. L. Wang, *Adv. Mater.* **2021**, *33*, 2102886; b) S. Lin, X. Chen, Z. L. Wang, *Chem. Rev.* **2022**, *122*, 5209.
[11] Y. Nan, J. Shao, M. Willatzen, Z. L. Wang, *Research* **2022**, *2022*, 9861463.
[12] a) S. Li, J. Nie, Y. Shi, X. Tao, F. Wang, J. Tian, S. Lin, X. Chen, Z. L. Wang, *Adv. Mater.* **2020**, *32*, 2001307; b) J. Nie, Z. Ren, L. Xu, S. Lin, F. Zhan, X. Chen, Z. L. Wang, *Adv. Mater.* **2020**, *32*, 1905696.
[13] S. Lin, C. Xu, L. Xu, Z. L. Wang, *Adv. Funct. Mater.* **2020**, *30*, 1909724.
[14] S. Lin, M. Zheng, J. Luo, Z. L. Wang, *ACS Nano* **2020**, *14*, 10733.
[15] a) X. Dong, Z. Wang, A. Berbille, X. Zhao, W. Tang, Z. L. Wang, *Nano Energy* **2022**, *99*, 107346; b) X. Zhao, Y. Su, A. Berbille, Z. L. Wang, W. Tang, *Nanoscale* **2023**, *15*, 6243.
[16] W.-Z. Song, M. Zhang, H.-J. Qiu, C.-L. Li, T. Chen, L.-L. Jiang, M. Yu, S. Ramakrishna, Z.-L. Wang, Y.-Z. Long, *Water Res.* **2022**, *226*, 119242.
[17] B. Chen, Y. Xia, R. He, H. Sang, W. Zhang, J. Li, L. Chen, P. Wang, S. Guo, Y. Yin, L. Hu, M. Song, Y. Liang, Y. Wang, G. Jiang, R. N. Zare, *Proc. Natl. Acad. Sci. USA* **2022**, *119*, e2209056119.
[18] M. Wang, S. Qiu, H. Yang, Y. Huang, L. Dai, B. Zhang, J. Zou, *Chemosphere* **2021**, *270*, 129448.
[19] a) T. Kakeshpour, A. Bax, *J. Magn. Reson.* **2021**, *333*, 107092; b) T. Kakeshpour, B. Metaferia, R. N. Zare, A. Bax, *Proc. Natl. Acad. Sci. USA* **2022**, *119*, e2121542119.
[20] a) S. A. Fischer, D. Gunlycke, *J. Phys. Chem. B* **2019**, *123*, 5536; b) L. Konermann, S. Kim, *J. Chem. Theory Comput.* **2022**, *18*, 3781; c) X. Wu, J. J. Hong, W. Shin, L. Ma, T. Liu, X. Bi, Y. Yuan, Y. Qi, T. W. Surta, W. Huang, J. Neuefeind, T. Wu, P. A. Greaney, J. Lu, X. Ji, *Nat. Energy* **2019**, *4*, 123; d) Q. Zhao, A. Song, W. Zhao, R. Qin, S. Ding, X. Chen, Y. Song, L. Yang, H. Lin, S. Li, F. Pan, *Angew. Chem., Int. Ed.* **2021**, *60*, 4169.
[21] a) D. Shao, L. Zhang, S. Sun, W. Wang, *ChemSusChem* **2018**, *11*, 527; b) W. Tian, J. Qiu, N. Li, D. Chen, Q. Xu, H. Li, J. He, J. Lu, *Nano Energy* **2021**, *86*, 106036; c) P. Wang, X. Li, S. Fan, X. Chen, M. Qin, D. Long, M. O. Tadé, S. Liu, *Appl. Catal., B* **2020**, *279*, 119340; d) G. Yin, C. Fu, F. Zhang, T. Wu, S. Hao, C. Wang, Q. Song, *J. Alloys Compd.* **2023**, *937*, 168382.
[22] a) J. Zhang, S. Lin, M. Zheng, Z. L. Wang, *ACS Nano* **2021**, *15*, 14830; b) X. Wang, J. Zhang, X. Liu, S. Lin, Z. L. Wang, *J. Mater. Chem. A* **2023**, *11*, 5696.
[23] L. L. Sun, S. Q. Lin, W. Tang, X. Chen, Z. L. Wang, *ACS Nano* **2020**, *14*, 17354.
[24] Z. L. Wang, A. C. Wang, *Mater. Today* **2019**, *30*, 34.
[25] G. Nardi, I. Manet, S. Monti, M. A. Miranda, V. Lhiaubet-Vallet, *Free Radic. Biol. Med.* **2014**, *77*, 64.
[26] L. Cao, C. Yang, B. Zhang, K. Lv, M. Li, K. Deng, *J. Hazard. Mater.* **2018**, *359*, 388.
[27] a) L. Qiu, R. G. Cooks, *Angew. Chem., Int. Ed.* **2022**, *61*, e202210765; b) J. Ma, F. Wang, M. Mostafavi, *Molecules* **2018**, *23*, 244.
[28] a) J. Staehelin, J. Hoigne, *Environ. Sci. Technol.* **1982**, *16*, 676; b) G. Merényi, J. Lind, S. Naumov, C. von Sonntag, *Chemistry* **2010**, *16*, 1372.
[29] a) Y. B. Vogel, C. W. Evans, M. Belotti, L. Xu, I. C. Russell, L.-J. Yu, A. K. K. Fung, N. S. Hill, N. Darwish, V. R. Gonçales, M. L. Coote, K. Swaminathan Iyer, S. Ciampi, *Nat. Commun.* **2020**, *11*, 6323; b) S. Ciampi, K. S. Iyer, *Curr. Opin. Electrochem.* **2022**, *34*, 100992.
[30] a) J. Xiong, Y. Liu, C. Li, Y. Zhou, F. Li, *Ultrason. Sonochem.* **2022**, *82*, 105899; b) L. Wolloch, J. Kost, *J. Control. Release* **2010**, *148*, 204.
[31] G. Kresse, J. Furthmüller, *Phys. Rev. B* **1996**, *54*, 11169.

